Designing Polymeric Interphases for Stable Lithium Metal Deposition

Sanjuna Stalin,[a‡] Mukul Tikekar,[b‡] Prayag Biswal,[a] Gaojin Li,[a] Hillis E. N. Johnson,[c] Yue Deng,[d] Qing Zhao,[a] Duylinh Vu,[a] Geoffrey W. Coates,[c] Lynden A. Archer*[a]

[a]School of Chemical and Biomolecular Engineering, Olin Hall, Cornell University, Ithaca, New York 14853, United States

[b]Sibley School of Mechanical and Aerospace Engineering, Upson Hall, Cornell University, Ithaca, New York 14853, United States

[c]Department of Chemistry and Chemical Biology, Cornell University, Baker Laboratory, Ithaca, New York 14853, United States

[d]Department of Materials Science and Engineering, Bard Hall, Cornell University, Ithaca, New York 14853, United States

[‡]These authors contributed equally

ABSTRACT: Reactive metals are known to electrodeposit with irregular morphological features on planar substrates. A growing body of work suggest that multiple variables — composition, mechanics, structure, ion transport properties, reductive stability, and interfacial energy of interphases formed either spontaneously or by design on the metal electrode play important but differentiated roles in regulating these morphologies. We examine the effect of fluorinated thermoset polymer coatings on Li deposition by means of experiment and theoretical linear stability analysis. By tuning the chemistry of the polymer backbone and sidechains, we investigate how physical and mechanical properties of polymeric interphases influence Li electrodeposit morphology. It is found that an interplay between elasticity and diffusivity leads to an optimum interphase thickness and that higher interfacial energy augments elastic stresses at a metal electrode to prevent out of plane deposition. These findings are explained using linear stability analysis of electrodeposition and provide guidelines for designing polymer interphases to stabilize metal electrodeposition.

Lithium batteries; Electrochemistry; Solid electrolyte interphases; Polymer Coatings; Stability Analysis; Operando-Microscopy

Rising demand for cost-effective and long-lasting rechargeable batteries has emerged as an important need in the transportation and electric power distribution sectors, particularly when renewable, intermittent technologies are used as low-carbon sources of electrical energy. Fundamental understanding of the formation mechanisms, mechanical stability, ion transport characteristics, and interfacial properties of solid-electrolyte interphases (SEI), typically formed spontaneously at battery anodes, though in its infancy is considered a requirement for progress.

The propensity of the Li metal anode to form non-planar, mossy structures (loosely termed *dendrites*) during battery recharge has been widely investigated in the literature.[1–4] It has been postulated that the formation of Li dendrites occurs in three stages[5] which involves formation of a heterogenous passivation layer followed by nucleation and growth of dendrites. This layer, termed the solid electrolyte interphase (SEI), was recently investigated by means of focused ion beam (FIB) cryo-genic SEM and electron spectroscopy techniques, and shown to be highly heterogeneous and far thicker than the analogous SEI formed on graphite anodes in lithium ion batteries (LIBs).[6–8] The heterogeneity of the SEI leads to hot spots with higher conductivity that nucleate the growth of dendrites, subsequently leading to convergence of electric field lines at the peaks of the nucleated dendrites that further facilitate their growth. This passivation layer continuously breaks and reforms by reaction with the electrolyte, promoting continuous growth of the dendrite into a ramified structure with the growth direction determined by the least reactive crystallographic facet of metallic Li.

Several approaches have been investigated to mitigate or, in rarer cases completely prevent the growth of lithium dendrites. These include salt additives to improve the properties of the SEI,[9,10] concentrated electrolytes,[11–14] single ion conductors [15,16] and high modulus electrolytes.[17–20] Tailoring the lithium metal/electrolyte interface with polymer coatings that serve as a protective barrier has gained attention in recent years. Recent studies have for example reported that interphases composed of self-healing polymers,[21] cross-linked polymers,[22,23] composites,[24] single ion conducting polymers,[25,26] and fluoropolymers[26,27] are effective in enabling high rate and high capacity deposition of lithium. Very few studies have attempted to elucidate how to design such polymer intherphases[28,29]. An emerging view is that fluorinated interphases enhance the reversibility of Li metal anodes and are essential for long term cycling stability of the Li anode, particularly in cases where the Li capacity in the battery anode and cathode are nearly balanced.[30–33] This has motivated multiple studies aimed at understanding the intrinsic physical and electrochemical characteristics of SEI enriched with Lithium Fluoride and other fluorinated compounds.[34–36]

Here, we consider design rules for elastic interphases formed on any generic metal anode and utilize experiments based on Li metal anodes to evaluate their effectiveness in arresting the various instabilities (*e.g.* morphological, chemical, mechanical/orphaning, and hydrodynamic) known to lower lifetime and reversibility of metal anodes.[5,37] By combining the experiments with theoretical stability analysis of metal electrodeposition across elastic interphases, we find that interphase thickness, mechanics, ion transport and interfacial properties all play precise, differentiated roles in setting the optimal interphase design. We focus specifically on thermosetting polymer interphases because their mechanical and chemical stability can be readily manipulated.

Thiol-Michael and thiol-ene reactions have been used in several reports to create functionalized cross-linked networks with tunable swelling and transport properties.[38–40] In this work, we synthesized fluorinated thiol cross-linkers according to a method previously reported by Nazrenko and coworkers (Figure 1(a)).[38,40] First, a methacrylate terminated fluoroalkyl monomer was added to pentaerythritol tetrakis(3-mercaptopropionate) in the presence of a nucleophilic catalyst (diethylamine). The methacrylate reacts with the thiol group through a thiol-Michael addition to produce a mixture of cross-linkers containing fluorinated side chains. By maintaining a 1:1 molar ratio between the fluoroalkyl monomer and the tetrathiol monomer, a statistical distribution favoring the monofunctionalized cross-linker was obtained. Therefore, we consider the average product to be a trifunctional cross-linker (3TF). The relative amount of fluorination of the networks was varied by tuning the length of the fluorinated sidechains, designated here as 3T3F, 3T7F and 3T10F. ^{1}H NMR (Figure S1) was used to monitor the disappearance of vinylic peaks near 6 ppm to confirm reaction completion.[38] The functionalized cross-linkers, along with (1,3,5-Triallyl-1,3,5-triazine-2,4,6(1H,3H,5H)-trione-3E) and a photoinitiator (benzophenone) were dissolved in a chloroform/ethanol (1:1 volume ratio) solvent mixture and spin-coated on polished stainless-steel substrates before UV-Curing to obtain coatings of different thicknesses, $\boldsymbol{h}$ .The parameters used to control $\boldsymbol{h}$ are reported in Table S1. Four $\boldsymbol{h}$ values (0.2, 2, 10 and 100 μm) using the cross-linker 3T10F were chosen for the initial study. The cured coatings were characterized by FT-IR (Figure S2) to confirm the disappearance of S–H and C=C peaks at ~2500 cm^{-1} and 1650 cm^{-1}, respectively. We evaluated the effect of $\boldsymbol{h}$ on ion-transport properties at the electrode/electrolyte interface using impedance spectroscopy at room temperature (Figure 1 (b)). The cells used for the measurements were composed of the coated polished stainless-steel electrodes and an O-ring filled with a liquid electrolyte (1M LiPF6 in EC/DMC) in the bulk (Scheme S1 (a)).

By fitting the spectra with an appropriate model (Scheme S1 (b), we can extract the individual bulk, coating, and charge transfer resistances. It is clear from Figure 1 (c) that most of the effect of $\boldsymbol{h}$ is restricted to the coating and charge transfer resistances; although at the highest h value the bulk resistance also seems to increase, possibly due to the fact that h and the inter electrode spacing are within the same order of magnitude. By performing temperature dependent impedance measurements and fitting the extracted coating and bulk resistances to the VFT equation ($\ln\frac{1}{\Omega} = \ln\frac{1}{\Omega_o} - \frac{\mathrm{E_a}}{\mathrm{R}(T-T_o)}$), we can extract the activation energy in the individual phases. The results reported in Figure 1 (d) indicate that the activation energy for ion transport in the coating is four times higher than that of bulk liquid electrolyte phase. The effect of $\boldsymbol{h}$ on the early stage deposition of Li was investigated by first depositing a small amount of lithium (0.1 mAh/cm2 at J = 1 mA/cm2), in (i) an ether based (1M LiTFSI in Diglyme) and (ii) a carbonate based (1M LiPF6 in EC/DMC) electrolyte. The nucleation overpotential, which is the first peak observed in the voltage response (Figure S3), increased with increasing $\boldsymbol{h}$ for both electrolytes as reported in Figure 2(b). This observation is consistent with expectations based on the impedance results. Scanning Electron Microscopy (SEM) was used to image the electrodes immediately after the end of the nucleation phase to analyze the lithium deposit size distribution. As reported in Figure 2(a), there is a significant difference in the lithium morphology under the influence of the coatings. The deposits are smaller, irregular and more three-dimensional in nature in the bare electrolyte case and under the influence of the coating, they are generally larger, flatter, and more two-dimensional for both electrolytes, which is the expected qualitative result if the interphase mechanics limit out-of-plane growth. Similar results are observed for electrodeposition of sodium (see Figure S8), implying that the origin of the observed effect is fundamental. Flatter and bigger metal electrodeposit nuclei have been reported to be beneficial for long-term operation and stability as these would grow into more planar deposits as compared to smaller nuclei. A more in-depth analysis of the SEM images provides additional information about how the deposit size and size distribution varies with $\boldsymbol{h}$. Results reported in Figure S4 & S5 show that the size distribution can be crudely fit to a normal distribution, indicating that while a large population of nuclei form at a certain time, a smaller population of nuclei may be developing at later times and growing independently during early stages of deposition.41,42 While the overpotential for deposition increases with h, surprisingly, the average deposit diameter (Figure 2(c)) is a decidedly non-monotonic function of h. The largest deposit is observed at an optimal h ≈ 2 μm, irrespective of the electrolyte.

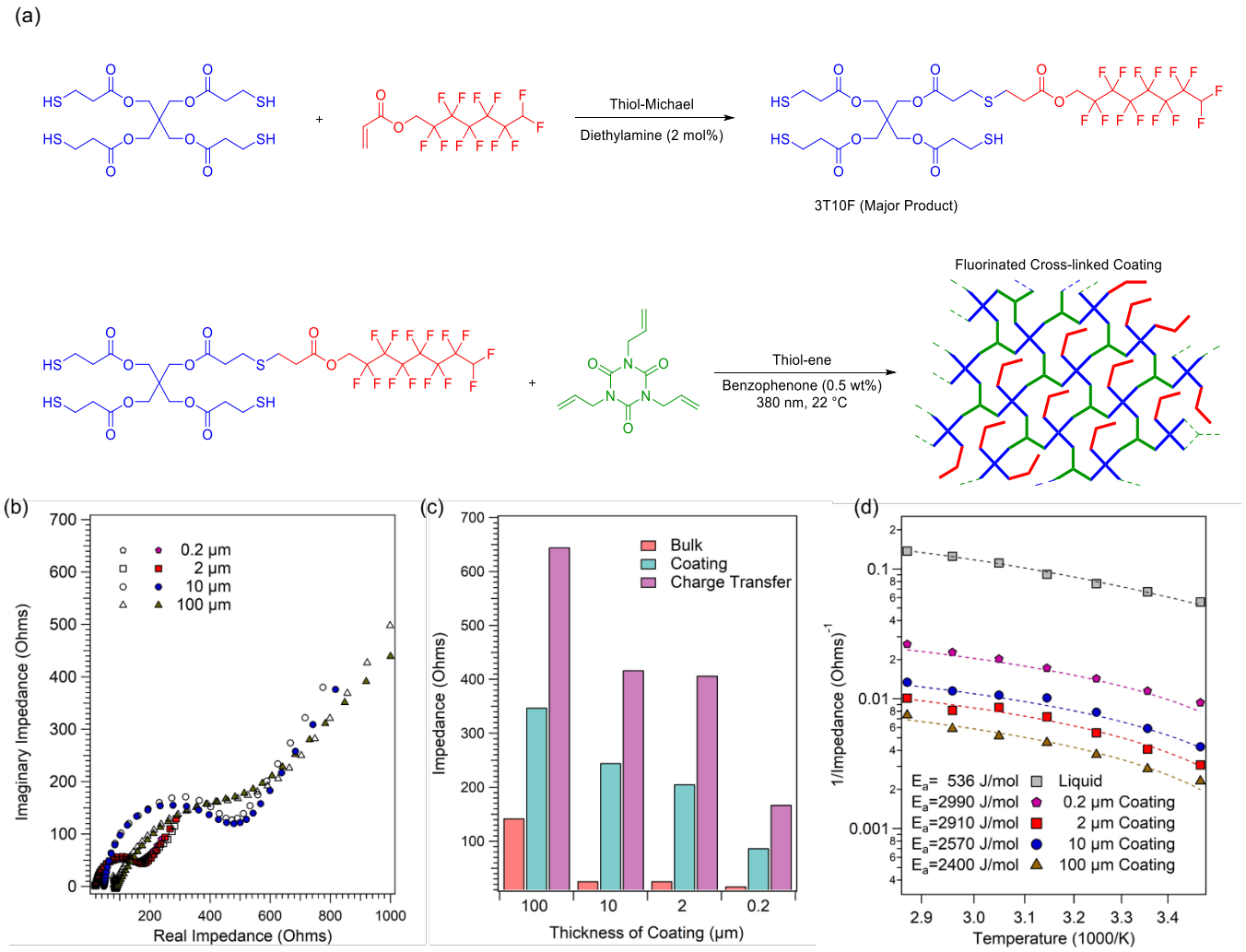

Figure 1: (a) Synthesis Scheme of fluorinated crosslinked polymer used in this study ; Effect of polymer ***h*** on Li^+ ion transport: (b) Impedance Spectra for polished electrodes with different h in combination with bulk electrolyte (1M $LiPF_6$ in EC/DMC) (c) Extracted Bulk, Coating and Charge transfer resistances (d) Temperature dependent measurements fitted with VFT equation and corresponding activation energies.

We note that while prior studies of polymer thin film mechanics have shown that mechanical strength rises with film thickness for nanometer-thick coatings,43–45 the large μm-scale thicknesses at which the optimum is observed imply that mechanics alone cannot be the source of the behavior. Figure 2(c) also includes a data set from a report28 that illustrates the effect of a Self-Healing Polymer on the average deposit size. We note that although these studies use a separator and a DOL/DME electrolyte, an optimum value of h is also observed.

In order to understand the source of the maximum and how the numerous design variables — mechanics, ion-transport characteristics, and interfacial properties — be used to create optimal interphases for any metal anode, we performed linear stability analysis for Li electrodeposition under an elastic interphase layer. The analysis is presented in detail as supplementary material in Section I of the Supporting Information. The methodology is similar to that reported in our previous study of Li electrodeposition in structured solid-state, bulk electrolytes.[3,46] Here, we summarize the methodology and key findings. Briefly, in our linear stability analysis we investigate how the growth rate σ of perturbations of prescribed wave length ($\lambda \equiv \pi/k$) or, equivalently wave number k, is influenced by changes to ***h***; shear modulus, G^s; cation diffusivity, D_c^i; salt concentration, C_{c0}, at the metal in the unperturbed state; current density J, and interfacial energy γ. For simplicity we model the coatings as simple Hookean elastic solids with Poisson ratio ν^m and consider the coating to be in equilibrium with a bulk liquid electrolyte with cation diffusivity, $D_c^o = D_c^i/D$, and a solid metal with molar volume v_m. Here D is termed the cation diffusivity ratio between the electrolyte bulk and interphase. For the case of a liquid electrolyte bulk and solid-state polymer interphase considered in the present study, $D \ll 1$. We solve Equations S-1:S-4 in the Supporting Information, in conjunction with the flux balance equations reported previously[46], subject to the boundary conditions S-5:S-7 to determine how small-amplitude perturbations of the Li electrode thickness shrink ($\sigma < 0$) or grow ($\sigma > 0$).

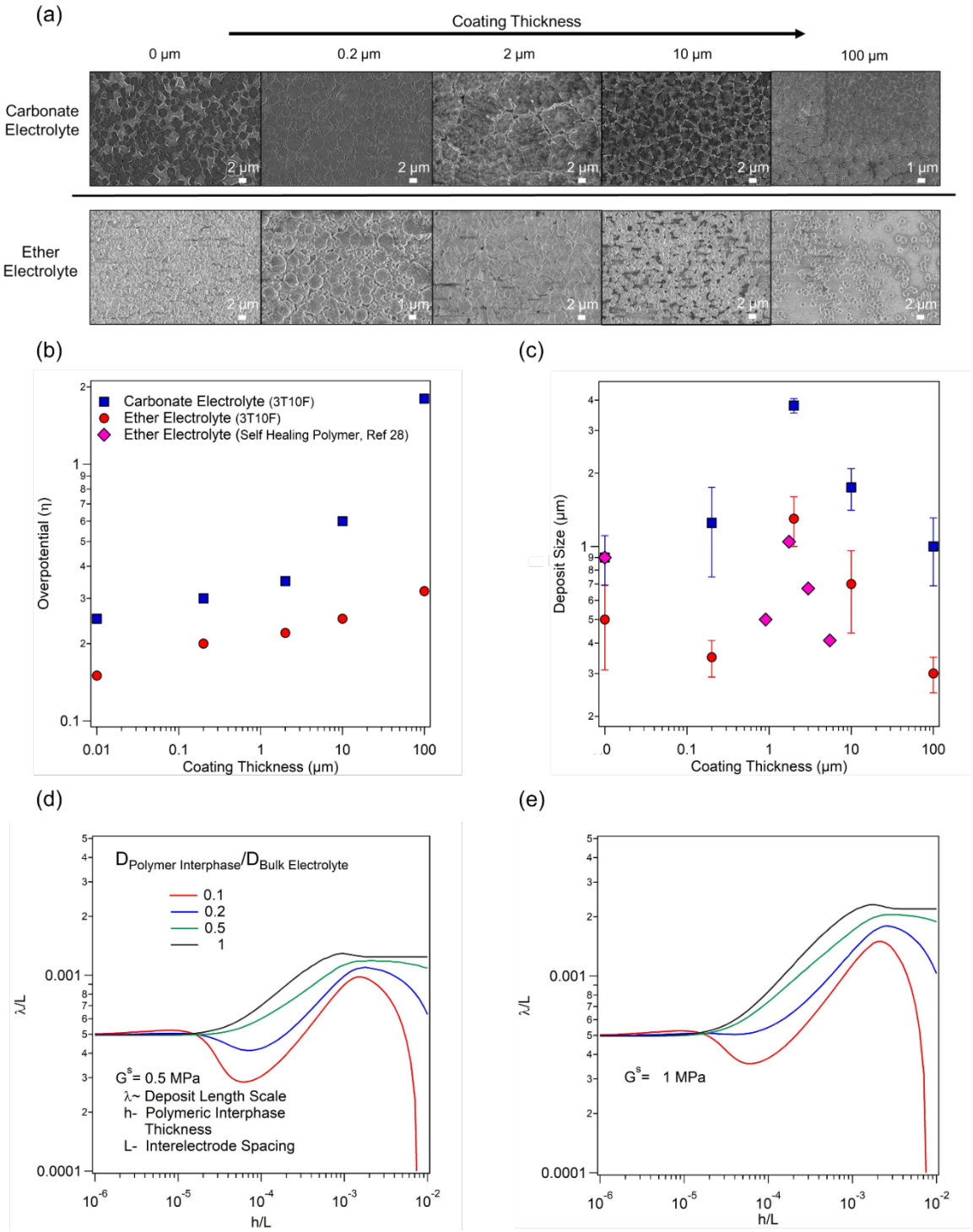

Figure 2: Effect of ***h*** on early stage growth of Lithium metal: (a) SEM images of deposits following nucleation event for two classes of electrolyte and different ***h*** values. (b) Nucleation overpotential measured under galvanostatic conditions for the two electrolytes as a function of ***h***. (c) The average deposit sizes for each ***h*** value obtained by first analyzing the full-size distribution using the ImageJ program, from which the mean value (points) and variance (error bars) were determined (Additional data set for Self-Healing Polymer from reference 31 has been included for comparison). Linear Stability Analysis reveals half-wavelength of the fastest growing mode as a function of ***h*** for various values of diffusivity contrast between the coating and liquid, in the case of (d) G^s = 0.5 MPa and (e) G^s = 1MPa.

When the wave number of electrode perturbations is much shorter than the interphase layer thickness, *i.e.* k$\boldsymbol{h}$ ≫1, the following analytical formula predicts how the growth rate is affected by the interphase properties and cell operating conditions,

$$\sigma = \frac{v_m}{F}[kJ - A(\gamma k^3 + 2G^s k^2)]$$

Here $A = \frac{D_c^i v_m F C_{c0}}{RT}\frac{2}{3}(1+\nu^m)$, and R, T and F are the gas constant, temperature and Faraday's constant respectively. In this limit, elastic stresses generated in the polymer coating decay completely over the thickness of the interfacial layer and the coating-outer liquid electrolyte-interface is undisturbed. The modulus of the polymer layer augments the surface tension ($k^3\gamma$) in stabilizing (making σ more negative) the deposition, but the effect is dependent on $\boldsymbol{h}$ through C_{c0}. The growth rate has a maximum at a wavenumber $k_{max} = \sqrt{\left(\frac{2}{3}\frac{G^s}{\gamma}\right)^2 + \frac{J}{3A\gamma}} - \frac{2}{3}\frac{G^s}{\gamma}$, which sets the half-wavelength, $\lambda^* \equiv \pi/k_{max}$, of the fastest growing mode. Thus, a larger interphase modulus and/or lower *J*, lowers k_{max}, which would favor deposition of larger electrodeposit structures. Likewise, we see that for a given polymer coating material and outer electrolyte chemistry (*i.e.* fixed G^s and γ), *J*, and in a situation when the polymer layer has a lower cationic diffusivity (i.e. $D < 1$), increasing $\boldsymbol{h}$ lowers the diffusion-limited current density, $J^* = \frac{4D_c^o FLC_0}{(L-\boldsymbol{h})^2}\left[\frac{\boldsymbol{h}(2L-h)D_c^o}{(L-\boldsymbol{h})^2 D_c^i} + 1\right]^{-1}$, which lowers C_{c0} and, A; reducing the size of the fastest growing mode. In comparison, when the interfacial film is much thinner than the wavelength of the electrode perturbation, *i.e.* $k\boldsymbol{h} \ll 1$, σ has a more complicated form,

$$\sigma = \frac{v_m}{F}\left[kJ\frac{D(1+k\boldsymbol{h})}{D+k\boldsymbol{h}} - \frac{D_c^i v_m F C_{c0}}{RT}\frac{2}{3}(1+\nu^m)\frac{1+k\boldsymbol{h}D}{D+k\boldsymbol{h}}\left(\gamma k^3 + \frac{G^s}{1-\nu^s}\boldsymbol{h}^3 k^5\right)\right]$$

Here the deformation of the film-liquid interface follows that of the metal-film interface. The effect of $\boldsymbol{h}$ on the half- wavelength of the fastest growing perturbation is plotted in Figure 2(d) and Figure 2(e). The sizes of the deposits are evidently influenced by the elasticity of the polymer layer only if the layer is thicker than $\boldsymbol{h} \gtrsim (\gamma^2 D_c^i v_m F C_0)^{1/3}/(JG^s RT)^{1/3}$. For coatings thinner than this limit, the primary mechanism for stabilizing the deposition is the interfacial energy of the metal-polymer interface, and the preferred wavelength is unaffected by $\boldsymbol{h}$. As $\boldsymbol{h}$ rises, elasticity starts to contribute more appreciably in stabilizing the deposition with the effect being highly nonlinear in thickness. For large $\boldsymbol{h}$, the elastic stresses completely decay over the film as discussed before and increasing the thickness further only adversely affects the stability of deposition due to higher resistance of the film. This trade-off is particularly noticeable as the diffusivity contrast between the coating and liquid increases and qualitatively explains the maximum in deposit size apparent in all the experimental results reported in Figure 2(a).

The maximum $\boldsymbol{h}$ for which interfacial energy alone stabilizes the metal deposition process [$\boldsymbol{h} \leq (\gamma^2 D_c^i v_m F C_0)^{1/3}/(JG^s RT)^{1/3}$], is approximately 150 nm for the conditions used in our experiments. Thus, for the values $\boldsymbol{h}$ used in the study, both surface tension and elasticity are controlling electrodeposit growth and stability. We next study how these two factors influence Li electrodeposition morphology. Lopez *et al* investigated the effect of surface energy of polymers on electrodeposition and concluded that lower surface energy favors more stable deposition.[28] Lower surface energy essentially results in high interfacial energy at the metal-polymer interface, which has a stabilizing effect. In order to systematically study this effect, four polymer coatings with varying degree of fluorination were created. The length of the fluorinated side chains in the first step was modified to yield monomers with different extents of fluorination before crosslinking. The functionalized thiol monomers 3T3F, 3T7F and 3T10F are shown in Figure 3(a). The cross-linked systems were characterized using Differential Scanning Calorimetry as shown in in Figure S6. The glass transition temperatures were found to decrease with increasing length of fluorine sidechain, possibly due to increase in free volume within the formed network. Lithiated Nafion was also included as a fourth polymer for comparison. Surface energy was calculated using contact angle measurements and Owens-Wendt method. Figure 3(b) reports SEM images of lithium deposits under the influence of different coatings. It is clear that the deposit size is correlated with the fluorine content of the polymer.[42] The measured surface energies were compared with the extracted nuclei sizes in Figure 3(c) and shows that lower surface energies result in larger deposit sizes.

The effect of J on the radius of Li deposits has been previously reported in detail for liquid electrolytes with and without additives.[41,42] Li deposited at the optimal $\boldsymbol{h}$ for the fluorinated polymer at different current densities was investigated using SEM (Figure S7). The nuclei sizes decreased with increasing *J*. It is also apparent that the deposit density increases with increasing *J*, with the distribution crudely fitting to a gaussian curve, indicating that the fluorinated polymeric interphase has a similar influence on the growth dynamics of the lithium deposits compared to an in-situ formed fluorinated interphase from additives like Fluoroethylene Carbonate (FEC).[42]

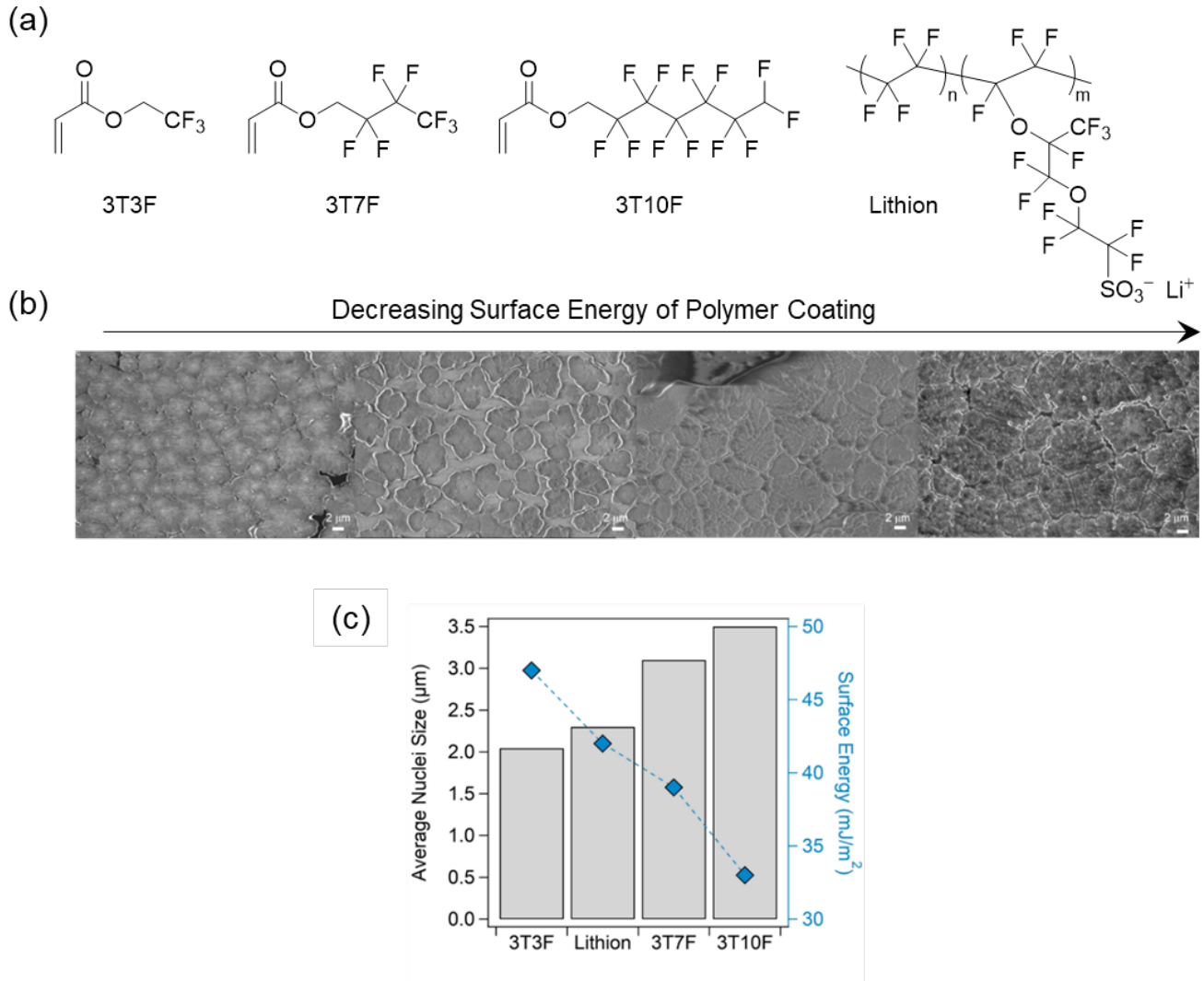

Figure 3: Effect of surface energy of polymer h on early stage growth of Lithium metal: (a) Structures of Lithiated Nafion and monomers used to functionalize thiol cross-linkers with different lengths of fluorinated sidechains. (b) SEM images of lithium deposits (0.1 mAh/cm^2 at 1 mA/cm^2) with carbonate electrolyte in bulk phase) under 3T3F, Lithion, 3T7F and 3T10F from left to right respectively. (c) Nuclei sizes for each case obtained from image analysis and surface energies calculated using contact angle measurements.

We also investigated Li electrodeposition in ether based cross-linked polymer (PEGDMA (M_w=450 g/mol) interphases with lower shear modulus (Figure S9) than the fluorinated networks. PEGDMA was included in the study because this coating chemistry is more widely used in the literature. Comparing its performance with those of the most promising fluorinated networks therefore provides an accessible, internally consistent benchmark for evaluating the fluorinated thermosets developed in the study. Physical properties of the ether-based coating are reported in Table S2 and impedance spectra in Figure S10. It is evident that the coating resistance is comparable to the fluorinated polymeric interphase. The value of ***h*** was also maintained as 2 µm in all cases.

Visualization of Li deposition was performed in a custom-designed apparatus and using optical microscopy. Figure 4(a) shows the results for J of 4 mA/cm^2. All cells used 1M $LiPF_6$ in EC/DMC as the bulk electrolyte. The average electrodeposit thickness was analyzed using Matlab to gain insight into the evolution of lithium electrodeposition. Multiple points on the propagating front were tracked and averaged to obtain plots of the deposit height and growth rate over time for the ether-based coating, fluorinated coating and no coating case. (Figure 4(b)). Comparing to what would be expected from a completely planar deposit, it is evident that the fluorinated polymer results in a close-to planar deposition of lithium metal, followed by the ether-based polymer which results in slightly higher values of deposit thickness. The deposited electrode surface was imaged by Scanning Electron Microscopy and confirms that the interphase mechanical shear modulus is an important variable in setting the deposit morphology (Figure 4(c)). Grazing Incidence X-Ray Diffraction (GIXRD) analysis was used to characterize the crystallography of the electrodeposited Li metal.[47,48] Figure 4(d) reports two dimensional GIXRD patterns for Li deposited on bare and fluoropolymer-coated (3T10F) polished stainless-steel substrates. A fixed deposit capacity of 5 mAh/cm^2, approximately 25µm of Li was used in both cases and no-separator was employed; the electrolyte was instead filled in an O-ring between the two electrodes. For lithium deposited on bare stainless steel, no diffractions associated with Li crystallites are detected. Considering the large amount of Li deposited, we conclude that much of the deposited lithium is either covered by a thick SEI or is dead lithium lost during

washing with solvent during sample preparation. For the lithium deposited on the coated substrate a clear and continuous (110) ring is detected. This indicates the integrity and freshness of the deposited lithium and a lack of anisotropy, possibly reflecting the grain boundaries observable in the deposited lithium. Thus, it can be inferred that the planarizing effect for the deposited metal in the growth regime increases with increasing elastic stresses at the electrode surface, consistent with theoretical results detailed above.

We evaluated the long-term electrochemical stability and reversibility of Li electrodeposition on substrates protected with fluorinated polymer interphases at the optimal ***h*** established in Figure 2. It is presumed that the polymer coating acts as a barrier to side reactions between the lithium metal and the bulk liquid electrolyte. To validate this hypothesis, chronoamperometry experiments were performed, whereby the cell was held at a fixed voltage (-50mV) to facilitate reduction reactions at the working electrode surface. A fixed amount of lithium (0.1 mAh/cm^2) was pre-deposited on coated and uncoated electrodes prior to testing and impedance of the cells were measured after potentiostatic holds at -50 mV for 1, 5 and 10 minutes. The extent of increase in impedance directly correlates to the extent of side reactions at the electrode.

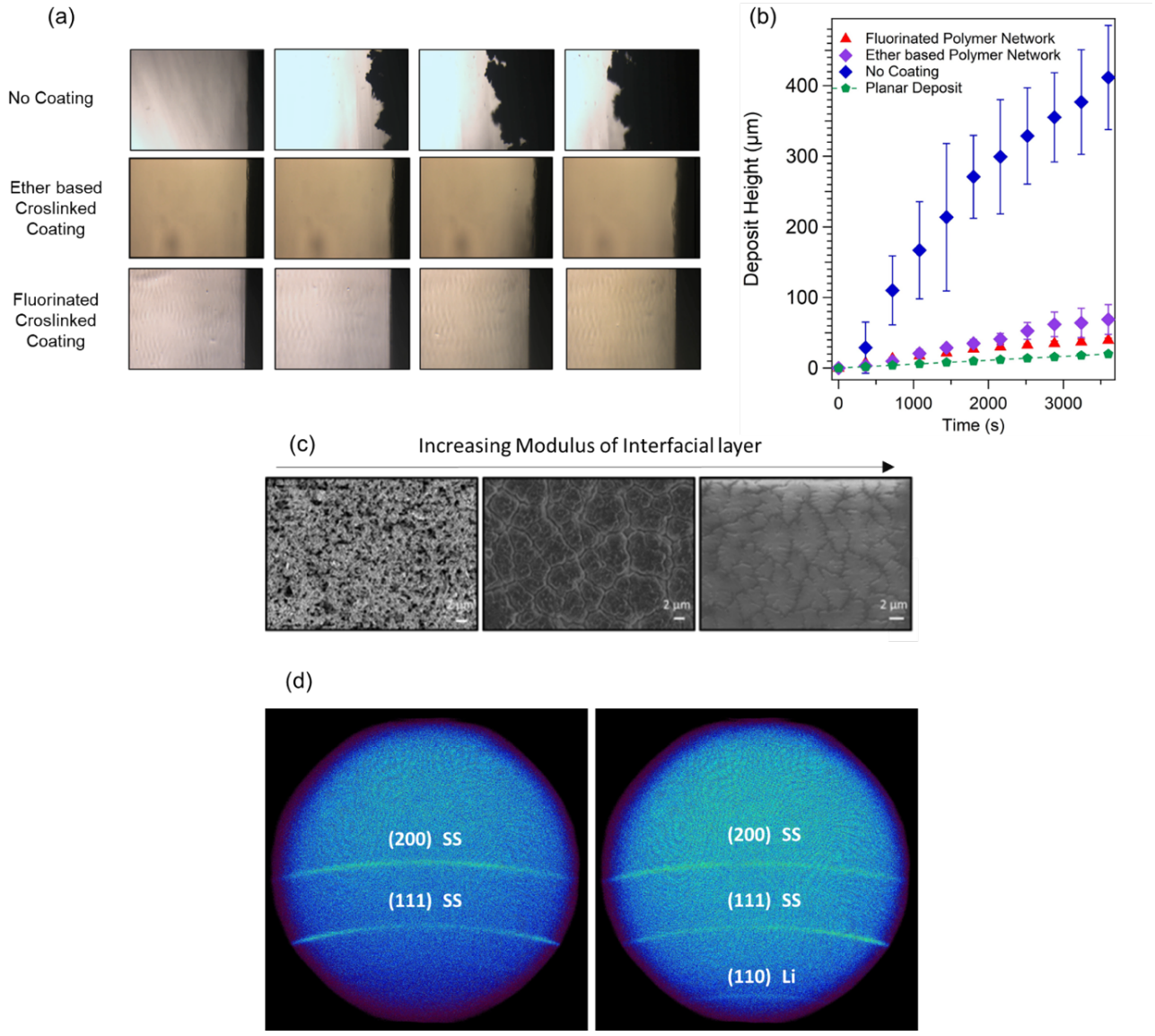

Figure 4: Visualization of lithium deposition in growth regime: (a) Snapshots of Li electrodeposit morphology from optical visualization studies (b) Growth rates extracted from time-dependent evolution of the electrodeposit thickness in (a);the error bars in the figure record variations in the deposit height or roughness, which is substantially reduced using polymer interphases of essentially any chemistry. (c) SEM images of electrode for no coating, polyether-based coating (PEGDMA), and fluorinated coating (3T10F) from left to right. (d) Grazing Incidence X-Ray Diffraction (GIXRD) analysis of Li deposited on bare stainless steel (SS) substrate (left) and on stainless steel substrate coated with 3T10F (right).

Figure 5(a)-(c) report the raw and fitted (Scheme 1(b)) impedance data. While the uncoated electrode has a lower initial impedance than that of the coated electrode for small periods of potentiostatic hold, as the time period increases, the interfacial impedance increases, indicating side reactions with the bulk electrolyte over time. In the case of the coated

electrode, the interfacial impedance shows no change to minimal change, thus supporting our hypothesis. This has important implications on long term stability of the anode, and in order to gain more insight, we measured coulombic efficiency of coated and bare anodes paired with different classes of electrolyte. We find that the coating significantly improves the lifetime of the cell, exceeding 400 cycles while maintaining a high coulombic efficiency of > 98%. Consistent with previous reports,[33] it was also found that the coulombic efficiency per cycle increased with increasing capacity of lithium, reaching around 98% for a capacity of 5 mAh/cm^2 (Figure S12). This further validate the coating's ability to host large amounts of lithium relevant for practical cell configurations.

Finally, to evaluate the practical relevance of the fluorinated polymer interphases in batteries, we created NCM 622 (Capacity~3.5 mAh/cm^2) - Li cells and studied their cycling behaviors under galvanostatic conditions. The anode used for these cells was created by lithiating polished stainless steel substrates (with/without the fluoropolymer coatings) to achieve anodes with Li capacity equal to that of the cathode (3 mAh/cm^2), in order to achieve a N:P ratio of around 1. It is worth noting that this is a more aggressive mode of testing the efficiency of full cells since there is an intrinsic porosity for the lithium formed via deposition as opposed to store-bought thin lithium anode. Figure S13(a) reports the capacity as a function of cycle number and Figure S13(b) reports the voltage profiles for the tenth cycle. The capacity retention in the full cells employing coated electrodes is superior to the uncoated case, consistent with our previous measurements and results.

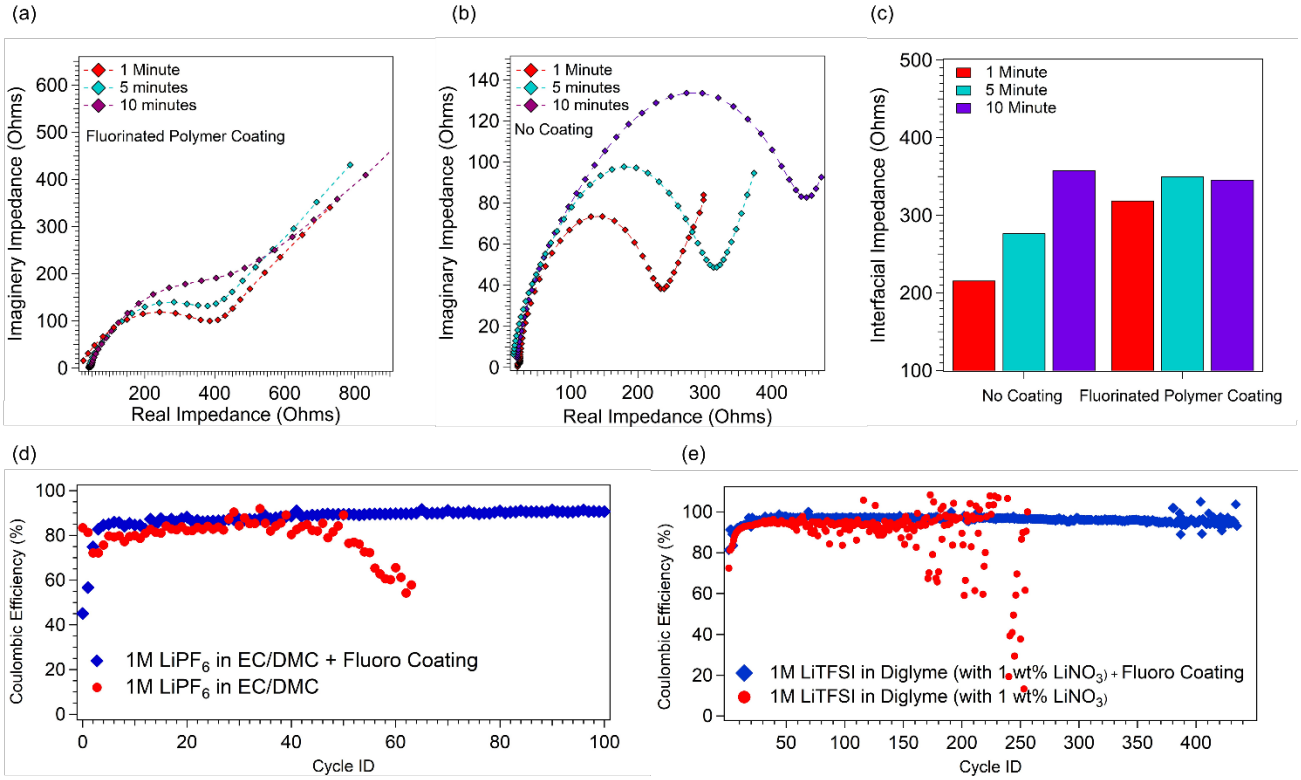

Figure 5: Electrochemical stability of fluorinated polymer interphases. Impedance measured after potentiostatic holds for different periods of time for: (a) coated electrodes; and (b) uncoated electrodes. (c) Interfacial impedance for coated and uncoated electrodes; (d) Coulombic efficiency versus cycle# in a carbonate electrolyte (J= 0.5 mA/cm^2, 1 mAh/cm^2). (e) Coulombic efficiency of cells with and without coated electrodes in an ether-based electrolyte (J= 0.5 mA/cm^2, 1 mAh/cm^2).

In summary, we studied the effect of elastic interphases on the stability of Li electrodeposition and found that the physical properties of fluoropolymer interphases have a profound effect on the deposit size at the initial stages of deposition; exhibiting an optimum thickness at which flatter deposit morphologies are favored. We theoretically show that this optimum reflects an interplay between elasticity and diffusivity. It can be readily manipulated using multiple, accessible material, interfacial, and electrochemical testing variables. Inspection of the theoretical expressions for the growth rate σ, both for $kh >> 1$ and $kh << 1$, also shows that there are numerous additional degrees of freedom available in designing these coatings. Our ongoing studies explore rational design of coatings with features predicted by theory and application of more precise characterization tools to evaluate the physical, mechanical, and electrochemical characteristics of the coatings. Additional studies designed to understand the effect of such polymeric interphases on Li electrodeposit morphology during the earliest nucleation phases and at different current densities of operation are vital for laying out the design principles for polymeric coatings that enable dendrite free metal anodes.

ASSOCIATED CONTENT

Supporting Information

Linear stability analysis, electrochemical analysis, and morphology are presented. Results from complementary SEM, Impedance

spectroscopy, and goniometer characterizations, coin cell fabrication, electrochemical testing methods, image analysis, and additional figures are included.

AUTHOR INFORMATION

Corresponding Author

*E-mail: laa25@cornell.edu

Author Contributions

‡These authors contributed equally.

ORCID

Sanjuna Stalin: 0000-0002-4786-6640
Hillis E. N. Johnson: 0000-0002-5998-9234
Qing Zhao: 0000-0003-0625-9892
Geoffrey W. Coates: 0000-0002-3400-2552
Lynden A. Archer: 0000-0001-9032-2772

Notes

The authors declare no competing financial interest.

ACKNOWLEDGMENT

The research was supported by the National Science Foundation, Partnerships for Innovation Program under award # IIP-1919013 and Beijing Institute of Collaborative Innovation. The electron microscopy facilities made use of the Cornell Center for Materials Research Shared Facilities which are supported through the NSF MRSEC program (DMR-1719875). The interface characterization work made use of the facilities available in CESI, Cornell.

REFERENCES

(1) Frenck, L.; Sethi, G. K.; Maslyn, J. A.; Balsara, N. P. Factors That Control the Formation of Dendrites and Other Morphologies on Lithium Metal Anodes. *Front. Energy Res.* **2019**, *7*, 115.

(2) Wood, K. N.; Kazyak, E.; Chadwick, A. F.; Chen, K. H.; Zhang, J. G.; Thornton, K.; Dasgupta, N. P. Dendrites and Pits: Untangling the Complex Behavior of Lithium Metal Anodes Through Operando Video Microscopy. *ACS Cent. Sci.* **2016**, *2*, 790–801.

(3) Zhang, X.; Wang, A.; Liu, X.; Luo, J. Dendrites in Lithium Metal Anodes: Suppression, Regulation, and Elimination. *Acc. Chem. Res.* **2019**, *11*, 3223–3232.

(4) Bai, P.; Li, J.; Brushett, F. R.; Bazant, M. Z. Transition of Lithium Growth Mechanisms in Liquid Electrolytes. *Energy Environ. Sci.* **2016**, *9*, 3221–3229.

(5) Tikekar, M. D.; Choudhury, S.; Tu, Z.; Archer, L. A. Design Principles for Electrolytes and Interfaces for Stable Lithium-Metal Batteries. *Nat. Energy* **2016**, *1*, 6–12.

(6) Li, Y.; Li, Y.; Pei, A.; Yan, K.; Sun, Y.; Wu, C. L.; Joubert, L. M.; Chin, R.; Koh, A. L.; Yu, Y.; Perrino, J.; Butz, B.; Chu, S.; Cui, Y. Atomic Structure of Sensitive Battery Materials and Interfaces Revealed by Cryo–Electron Microscopy. *Science* **2017**, *358*, 506–510.

(7) Zachman, M. J.; Tu, Z.; Archer, L. A.; Kourkoutis, L. F. Probing the Native Structure and Chemistry of Dendrites and SEI Layers in Li-Metal Batteries by Cryo-FIB Lift-Out and Cryo-STEM. *Microsc. Microanal*. **2018**, *24*, 1518–1519.

(8) Zachman, M. J.; Tu, Z.; Choudhury, S.; Archer, L. A.; Kourkoutis, L. F. Cryo-STEM Mapping of Solid–Liquid Interfaces and Dendrites in Lithium-Metal Batteries. *Nature* **2018**, *560*, 345–349.

(9) Zheng, J.; Engelhard, M.H.; Mei, D.; Jiao, S.; Polzin, B.J.; Zhang, G.J.; Xu, W. Electrolyte Additive Enabled Fast Charging and Stable Cycling Lithium Metal Batteries. *Nat. Energy* **2017**, *2*, 17012.

(10) Lu, Y.; Tu, Z.; Archer, L. A. Stable Lithium Electrodeposition in Liquid and Nanoporous Solid Electrolytes. *Nat. Mater*. **2014**, *13*, 961–969.

(11) Yu, J.; Gao, N.; Peng, J.; Ma, N.; Liu, X.; Shen, C.; Xie, K.; Fang, Z. Concentrated LiODFB Electrolyte for Lithium Metal Batteries. *Front. Chem*. **2019**, *7*, 494.

(12) Yu, L.; Chen, S.; Lee, H.; Zhang, L.; Engelhard, M.H.; Li, Q.; Jiao, S.; Liu, J.; Xu, W.; Zhang, J.G. A Localized High-Concentration Electrolyte with Optimized Solvents and Lithium Difluoro(oxalate)borate Additive for Stable Lithium Metal Batteries. *ACS Energy Lett*. **2018**, *3*, 2059–2067.

(13) Suo, L.; Borodin, O.; Gao, T.; Olguin, M.; Ho, J.; Fan, X.; Luo, C.; Wang, C.; Xu, K. 'Water-in-salt' Electrolyte Enables High-Voltage Aqueous Lithium-ion Chemistries. *Science* **2015**, *350*, 938–943.

(14) Qian, J.; Henderson, W. A.; Xu, W.; Bhattacharya, P.; Engelhard, M.; Borodin, O.; Zhang, J. G. High Rate and Stable Ccycling of Lithium Metal Anode. *Nat. Commun*. **2015**, *6*, 6362.

(15) Bouchet, R.; Maria, S.; Meziane, R.; Aboulaich, A.; Lienafa, L.; Bonnet, J. P.; Phan, T. N. T.; Bertin, D.; Gigmes, D.; Devaux, D.; Denoyel, R.; Armand, M. Single-ion BAB Triblock Copolymers as Highly Efficient Electrolytes for Lithium-Metal Batteries. *Nat. Mater.* **2013**, *12*, 452–457.

(16) Schaefer, J. L.; Yanga, D. A.; Archer, L. A. High Lithium Transference Number Electrolytes Via Creation of 3-Dimensional, Charged, Nanoporous Networks from Dense Functionalized Nanoparticle Composites. *Chem. Mater.* **2013**, *25*, 834–839.

(17) Duan, H.; Yin, Y. X.; Shi, Y.; Wang, P. F.; Zhang, X.; Yang, C.; Shi, J.; Wen, R.; Guo, Y.; Wan, L. Dendrite-Free Li-Metal Battery Enabled by a Thin Asymmetric Solid Electrolyte with Engineered Layers. *J. Am. Chem. Soc.* **2018**, *140*, 82–85.

(18) Choudhury, S.; Stalin, S.; Deng, Y.; Archer, L. A. Soft Colloidal Glasses as Solid-State Electrolytes. *Chem. Mater.* **2018**, *30*, 5996–6004.

(19) Khurana, R.; Schaefer, J. L.; Archer, L. A.; Coates, G. W. Suppression of Lithium Dendrite Growth Using Cross-Linked Polyethylene/Poly(Ethylene Oxide) Electrolytes: A New Approach for Practical Lithium-Metal Polymer Batteries. *J. Am. Chem. Soc.* **2014**, *136*, 7395–7402.

(20) Zhou, W.; Wang, S.; Li, W.; Xin, S.; Manthiram, A.; Goodenough, J.B. Plating a Dendrite-Free Lithium Anode with a Polymer/Ceramic/Polymer Sandwich Electrolyte. *J. Am. Chem. Soc.* **2016***, 138,* 9385–9388.

(21) Zheng, G.; Wang, C.; Pei, A.; Lopez, J.; Shi, F.; Chen, Z.; Sendek, A. D.; Lee, H.; Lu, Z.; Schneider, H.; Safont-Sempere, M. M.; Chu, S.; Bao, Z.; Cui, Y. High-Performance Lithium Metal Negative Electrode with a Soft and Flowable Polymer Coating. *ACS Energy Lett.* **2016**, *1*, 1247–1255.

(22) Choudhury, S.; Stalin, S.; Vu, D.; Warren, A.; Deng, Y.; Biswal, P.; Archer, L. A. Solid-State Polymer Electrolytes for High-Performance Lithium Metal Batteries. *Nat. Commun.* **2019**, *10*, 1–8.

(23) Yu, Z.; Mackanic, D. G.; Michaels, W.; Lee, M.; Pei, A.; Feng, D.; Zhang, Q.; Tsao, Y.; Amanchukwu, C. V.; Yan, X.; Wang, H.; Chen, S.; Liu, K.; Kang, J.; Qin, J.; Cui, Y.; Bao, Z. A Dynamic, Electrolyte-Blocking, and Single-Ion-Conductive Network for Stable Lithium-Metal Anodes. *Joule* **2019**, *3*, 2761–2776.

(24) Liu, Y.; Lin, D.; Yuen, P. Y.; Liu, K.; Xie, J.; Dauskardt, R. H.; Cui, Y.; An Artificial Solid Electrolyte Interphase with High Li-Ion Conductivity, Mechanical Strength, and Flexibility for Stable Lithium Metal Anodes. *Adv. Mater.* **2017**, *29*, 1605531.

(25) Ma, L.; Fu, C.; Li, L.; Mayilvahanan, K. S.; Watkins, T.; Perdue, B. R.; Zavadil, K. R.; Helms, B. A. Nanoporous Polymer Films with a High Cation Transference Number Stabilize Lithium Metal Anodes in Light-Weight Batteries for Electrified Transportation. *Nano Lett.* **2019**, *19*, 1387–1394.

(26) Tu, Z.; Choudhury, S.; Zachman, M. J.; Wei, S.; Zhang, K.; Kourkoutis, L. F.; Archer, L. A. Designing Artificial Solid-Electrolyte Interphases for Single-Ion and High-Efficiency Transport in Batteries. *Joule* **2017**, *1*, 394–406.

(27) Luo, J; Fang, C. C.; Wu, N. L. High Polarity Poly(vinylidene difluoride) Thin Coating for Dendrite-Free and High-Performance Lithium Metal Anodes. *Adv. Energy Mater.* **2018**, *8*, 1701482.

(28) Lopez, J.; Pei, A.; Oh, J. Y.; Wang, J. G.; Cui, Y.; Bao, Z. Effects of Polymer Coatings on Electrodeposited Lithium Metal. *J. Am. Chem. Soc.* **2018**, *140*, 11735–11744.

(29) Kong, X.; Rudnicki, P. E.; Choudhury, S.; Bao, Z.; Qin, J. Dendrite Suppression by a Polymer Coating: A Coarse-Grained

Molecular Study. *Adv. Funct. Mater.* **2020**, *Early View*, 1910138.
(30) Choudhury, S.; Archer, L. A. Lithium Fluoride Additives for Stable Cycling of Lithium Batteries at High Current Densities. *Adv. Electron. Mater.* **2015**, *2*, 1500246.
(31) Li, T.; Zhang, X. Q.; Shi, P.; Zhang, Q. Fluorinated Solid-Electrolyte Interphase in High-Voltage Lithium Metal Batteries. *Joule* **2019**, *3*, 2647–2661.
(32) Pathak, R.; Chen, K.; Gurung, A.; Reza, K. M.; Bahrami, B.; Pokharel, J.; Baniya, A.; He, W.; Wu, F.; Zhou, Y.; Xu, K.; Qiao, Q. Fluorinated Hybrid Solid-Electrolyte-Interphase for Dendrite-Free Lithium Deposition. *Nat. Commun.* **2020**, *11*, 93.
(33) Zheng, J.; Tang, T.; Zhao, Q.; Liu, X.; Deng, Y.; Archer, L. A. Physical Orphaning versus Chemical Instability: Is Dendritic Electrodeposition of Li Fatal? *ACS Energy Lett.* **2018**, *4*, 1349–1355.
(34) He, M.; Guo, R.; Hobold, G. M.; Gao, H.; Gallant, B. M. The Intrinsic Behavior of Lithium Fluoride in Solid Electrolyte Interphases on Lithium. *Proc. Natl. Acad. Sci. U. S. A.* **2020**, *117*, 73–79.
(35) Ko, J.; Yoon, Y. S. Recent Progress in LiF Materials for Safe Lithium Metal Anode of Rechargeable Batteries: Is LiF the Key to Commercializing Li Metal Batteries? *Ceram. Int.* **2019***, 45*, 30–49.
(36) Suo, L.; Xue, W.; Gobet, M.; Greenbaum, S. G.; Wang, C.; Chen, Y.; Yang, W.; Li, Y.; Li, J. Fluorine-Donating Electrolytes Enable Highly Reversible 5-V-Class Li Metal Batteries. *Proc. Natl. Acad. Sci. U. S. A.* **2018**, *115 (6)*, 1156–1161.
(37) Cheng, X. B.; Zhang, R.; Zhao, C. Z.; Zhang, Q. Toward Safe Lithium Metal Anode in Rechargeable Batteries: A Review. *Chem. Rev.* **2017**, *117 (15)*, 10403–10473.
(38) Goetz, J. T.; Nazarenko, S. Fluorine Containing UV-Curable Materials for Advanced Transport Applications. Ph. D. Thesis, University of Southern Mississippi, **2014**.
(39) Stalin, S.; Johnson, H. E. N.; Biswal, P.; Vu, D.; Zhao, Q.; Yin, J.; Abel, B. A.; Deng, Y.; Coates, G. W.; Archer, L. A. Achieving Uniform Lithium Electrodeposition in Cross-linked Poly(ethylene oxide) Networks: Soft Polymers Prevent Metal Dendrite Proliferation. *Submitted*
(40) Xiong, L.; Kendrick, L. L.; Heusser, H.; Webb, J. C.; Sparks, B. J.; Goetz, J. T.; Guo, W.; Stafford, C. M.; Blanton, M. D.; Nazarenko, S.; Patton, D. L. Spray-Deposition and Photopolymerization of Organic-Inorganic Thiol-ene Resins for Fabrication of Superamphiphobic Surfaces. *ACS Appl. Mater. Interfaces* **2014***, 6(13)*, 10763–10774.
(41) Pei, A.; Zheng, G.; Shi, F.; Li, Y.; Cui, Y. Nanoscale Nucleation and Growth of Electrodeposited Lithium Metal. **2017**, *17*, 1132–1139.
(42) Biswal, P.; Stalin, S.; Kludze, A.; Choudhury, S.; Archer, L. A. On the Nucleation and Early-Stage Growth of Li Electrodeposits. *Nano Lett.* **2019**, *19*, 8191–8200.
(43) O'Connell, P. A.; McKenna, G. B. Rheological Measurements of the Thermoviscoelastic Response of Ultrathin Polymer Films. *Science* **2005**, *307*, 1760–1763.
(44) Ao, Z.; Li, S. Temperature- and Thickness-Dependent Elastic Moduli of Polymer Thin Films. *Nanoscale Res. Lett.* **2011**, *6*, 1–6.
(45) Chang, J.; Toga, K. B.; Paulsen, J. D.; Menon, N.; Russell, T. P. Thickness Dependence of the Young's Modulus of Polymer Thin Films. *Macromolecules* **2018**, *51(17)*, 6764–6770.
(46) Tikekar, M. D.; Archer, L. A.; Koch, D. L. Stabilizing Electrodeposition in Elastic Solid Electrolytes Containing Immobilized Anions. *Sci. Adv.* **2016**, *2*, 7.
(47) Zheng, J.; Zhao, Q.; Tang, T.; Yin, J.; Quilty, C. D.; Renderos, G. D.; Liu, X.; Deng, Y.; Wang, L.; Bock, D. C.; Jaye, C.; Zhang, D.; Takeuchi, E. S.; Takeuchi, K. J.; Marschilok, A. C.; Archer, L. A. Reversible Epitaxial Electrodeposition of Metals in Battery Anodes. *Science* **2019**, *366*, 645–648.
(48) Shi, F.; Pei, A.; Vailionis, A.; Xie, J.; Liu, B.; Zhao, J.; Gong, Y.; Cui, Y. Strong Texturing of Lithium Metal in Batteries. *Proc. Natl. Acad. Sci. U. S. A.* **2017**, *114*, 12138–12143.

TOC Graphic

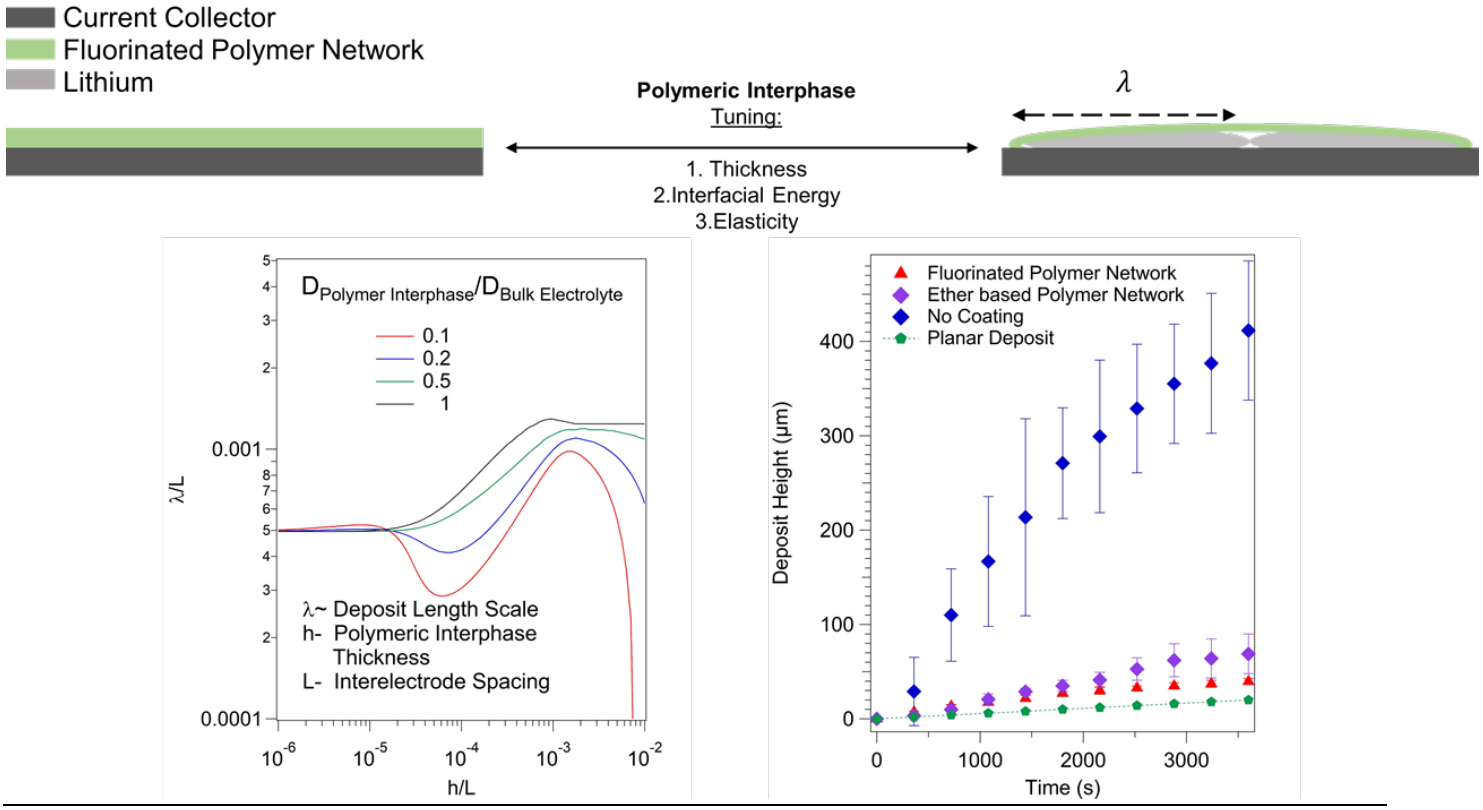
Current Collector
Fluorinated Polymer Network
Lithium
Polymeric Interphase
Tuning:
1. Thickness
2.Interfacial Energy
3.Elasticity
λ
$D_{Polymer\ Interphase}/D_{Bulk\ Electrolyte}$
0.1
0.2
0.5
1
λ/L
h/L
λ~ Deposit Length Scale
h- Polymeric Interphase Thickness
L- Interelectrode Spacing
Fluorinated Polymer Network
Ether based Polymer Network
No Coating
Planar Deposit
Deposit Height (μm)
Time (s)